200830026A

別紙1

厚生労働科学研究費補助金

エイズ対策研究事業

AZT誘発ミトコンドリア機能障害に対する分子治療方法の開発

平成20年度　総括研究報告書

研究代表者　佐藤　岳哉

平成２１（２００９）年　４月

別紙２

目　　次

別紙３

厚生労働科学研究費補助金（エイズ対策研究事業）
総括研究報告書
AZT誘発ミトコンドリア機能障害に対する分子治療方法の開発

研究代表者　佐藤　岳哉　東北大学大学院医学系研究科・助教

研究要旨：抗 HIV 薬のアジドチミジン(AZT)は、HIV に対する有効な作用を発揮する。その反面、重篤な副作用、心筋ミオパチーを誘発するが、その分子機構は不明である。今年度、AZT 代謝に関与する酵素チミジル酸キナーゼ(tmpk)の変異型を発現するラット心筋培養細胞を用いて、AZT の細胞に対する効果を検討した。種々の検討の結果、AZT 代謝物のうち活性化体である AZT3 リン酸がミトコンドリア機能障害を強く誘発することが明らかとなった。

分担研究者　柳澤　輝行
東北大学大学院医学系研究科・教授

A. 研究目的

抗 HIV 薬として用いられているアジドチミジン(AZT)代謝物が誘発するミトコンドリア機能障害の詳細な分子機構の詳細な解析から、ミトコンドリア機能障害を誘発する責任分子(群)すなわち AZT 代謝物が標的とする分子(群)を同定することを目的とする。さらにこの副作用を持たない新規薬物、あるいは、副作用に対する保護作用を示す薬物をスクリーニングすることにより、HAART 治療における AZT 誘発ミトコンドリア機能不全症を防ぐ分子標的薬の開発を目指す。

B. 研究方法

昨年度、作成したラット心筋由来細胞 H9c2 に AZT 代謝に関与するチミジル酸キナーゼ(Tmpk)の野生型あるいは変異型 cDNA を導入した細胞を用いた。まず、これらの細胞における tmpk 遺伝子の発現を確認するために、ドイツ Maxplank 研究所の Konrad 博士から提供された抗ヒト tmpk 抗体を用いる Western blot 法による解析を行った

次に、上記細胞の AZT 感受性を種々の濃度の AZT 存在下で 4 日間培養後、ATP 量を Cell Titer Glo キット (Promega)を用いて定量した。さらに AZT 処置後に細胞内に蓄積する AZT 代謝物のミトコンドリア機能に対する影響を検討するために、1 mM 存在下、4 日間培養した細胞をミトコンドリア内膜の膜電位感受性の蛍光プローブ JC-1 を用いて染色後、JC-1 の蛍光強度を蛍光プレートリーダーを用いて測定した。ミトコンドリア機能障害が起きると細胞は、アポトーシスを起こすことが知られている。そこで、AZT 処置後の細胞においてアポトーシスが起きているかどうかについて、アポトーシスの初期に細胞膜表面に発現が増加するホスファチジルセリンに特異的に結合する蛍光標識アネキシン V を用いて、細胞を染色し、細胞に結合したアネキシン V の蛍光強度をフローサイトメトリにより測定を行った。

（倫理面への配慮）

本研究において、倫理面において配慮が必要とされる研究は行わない。また、本研究においては、安全対策を必要とするレンチウィルスベクターの使用が含まれているが、申請者らはすでにこのウィルスベクター系を使うことに対する十分な安全対策を施した遺伝子組み換え実験計画を東北大学

遺伝子組換え実験安全専門委員会に申請し、承認済みである。この試験計画を試行するにあたり、試験に使用した大腸菌、細胞および組換え DNA 分子は、オートクレーブ等により不活化して廃棄する。

C. 研究結果

(1) 遺伝子導入細胞における導入遺伝子発現の確認

レンチウィルスベクターを用いて、tmpk 遺伝子を導入した H9c2 細胞における導入遺伝子の発現をウサギ抗ヒト tmpk 抗体を用いる Western blot 法で確認した。非遺伝子導入細胞である親株の細胞では、ヒト tmpk の発現は、確認されなかったのに対し、tmpk 野生型あるいは変異型遺伝子を導入した細胞においては、ヒト tmpk の分子量に相当するタンパク質のバンドが確認された。

(2) AZT 処置後の ATP 量の変化の検討

Tmpk 変異型遺伝子発現細胞においては、AZT 濃度依存的な ATP 量の減少が観察されたが、対照群（親株、および tmpk 野生型遺伝子発現細胞）では、それがみられなかった。また、tmpk 変異型遺伝子導入細胞は、10 μM 以上の濃度の AZT 添加により、AZT 濃度依存性かつ時間依存的な顕著な細胞内 ATP 量の減少がみられた。一方、対照群では、100 μM 以上の AZT 存在下において、有意な細胞内 ATP 量の低下が観察された。以上より、tmpk 変異型遺伝子発現細胞は、AZT 感受性が対照群よりも亢進していることを確認した。

(3) AZT 処置後のミトコンドリア膜電位変化の検討

1 mM AZT 存在下、4 日間培養した細胞を JC-1 で染色し、JC-1 の蛍光強度を測定した。Tmpk 変異型遺伝子発現細胞においては、AZT 処置により顕著なミトコンドリア内膜の膜電位低下が認められた。一方、対照群ではそれが認められなかった。

(4) AZT 処置後のアポトーシス誘導に関する検討

1 mM AZT 存在下、4 日間培養した細胞についてアポトーシスの誘導を検討した。Tmpk 変異型遺伝子発現細胞では、AZT 処置によるアポトーシス誘導が未処置細胞に比して顕著かつ有意な亢進を示した。それに対し、対照群の細胞のうち、tmpk 野生型細胞を AZT 処置後のアポトーシス誘導は親株のそれよりも増加傾向が見られたが、有意ではなかった。

D. 研究結果

Tmpk 遺伝子導入を行った細胞では、導入遺伝子の発現が確認された。親株における内在性 tmpk の発現は確認されなかったが、これは用いた抗体の特異性（ヒト tmpk 特異的）によるものと考えている。

Tmpk 遺伝子発現細胞を 1 mM AZT 存在下で 4 日間培養後、細胞内 ATP 量を測定したところ、tmpk 変異体遺伝子発現細胞において、ATP 量の顕著な低下がみられたのに対し、対照群ではそれがみられなかった。これは、発現させた tmpk 変異体蛋白質により、AZT が活性化体 AZT 三リン酸(AZTTP)へ変換され、ミトコンドリア機能障害を誘発したためと考えられた。これを確認するために、AZT 処置後の細胞におけるミトコンドリア機能障害の指標としてミトコンドリア膜電位を測定した。Tmpk 変異型遺伝子発現細胞においては、AZT 処置により顕著なミトコンドリア内膜の膜電位低下が認められた。一方、対照群ではそれが認められなかった。これは AZT 代謝物のうち AZTTP が、対照群の細胞において蓄積すると考えられる AZT 中間代謝物 AZT 一リン酸(AZTMP)よりもミトコンドリア機能を強く障害することを示すものである。この AZT 代謝物蓄積によるミトコンドリア機能障害の分子機構については、AZT 処置後に細胞内に活性酸素分子種産生が亢進するという予備データが得られており、次年度においてはこれについて詳細に検討し、AZT 誘発ミトコンドリア機能障害の分子機構を証明したいと考えている。さらに AZT 処置によりミトコンドリア機能障害が誘発されると、細胞のアポトーシスが進行すると考えて、AZT 処置後の初期アポトーシス亢進につ

いて検討した。その結果、予測したとおり Tmpk 変異型遺伝子発現細胞においては、AZT 処置により有意かつ顕著なアポトーシス亢進が認められた。一方、対照群ではそれが認められなかった。これらの結果から、AZT 誘発ミトコンドリア機能障害において、AZT 代謝物のうち、AZTTP が AZTMP よりも強くそれを誘導するということが明らかになった。従来は、AZT 代謝物のうち AZTMP がミトコンドリア機能障害を誘発すると考えられていた。しかしながら、今回確立した細胞系を用いた検討では、それとは異なる結果を得た。現在の評価に要する時間は、約 4 日であるが、従来の AZT 代謝物の影響を評価する際には 1 カ月以上の時間を必要とした。今回の検討結果と、従来の評価結果を比較、検討を行うためには、本細胞系を用い、より低濃度 AZT 処置後のより長期のミトコンドリア機能障害について検討をする必要がある可能性があると考えている。

E. 結論

確立した tmpk 遺伝子発現 H9c2 細胞は、AZT 代謝物誘発ミトコンドリア機能障害およびアポトーシス誘導の分子機構を詳細に検討することができる有用なものであるということが明らかとなった。今後、これを用いて AZT などの NRTI により誘発される心筋ミオパチーの詳細な分子機構の検討および、その研究成果に基づく分子標的予防方法についての開発を進めていく必要がある。

F. 健康危険情報

特になし

G. 研究発表

1．論文発表

(1) Higuchi K, Ayach B, **Sato T**, Chen M, Devine SP, Rasaiah VI, Dawood F, Yanagisawa T, Tei C, Takenaka T, Liu PP, Medin JA. Direct Injection of Kit Ligand-2 Lentivirus Improves Cardiac Repair and Rescues Mice Post-myocardial Infarction. Mol. Ther. 17 (2),262-268, 2009.

(2) Maeda K, Haraguchi M, Kuramasu A, **Sato T**, Ariake K, Sakagami H, Kondo H, Yanai K, Fukunaga K, Yanagisawa T, Sukegawa J. CLIC4 interacts with histamine H3 receptor and enhances the receptor cell surface expression. Biochem Biophys Res Commun. 369 (2), 603-608, 2008.

2. 口頭発表

1) Bystander killing highlights the utility of the tmpkF105Y/AZT system for suicide gene therapy of cancer.
Takeya Sato, Anton Neschadim, Jun Sukegawa, Teruyuki Yanagisawa, Jeffrey A. Medin.
第 11 回アメリカ遺伝子治療学会年会、2008 年 5 月 28 日～6 月 1 日 Boston, USA.

2) Thymidylate kinase over-expressing cells showed the mitochondrial myopathy by anti-HIV drug.
Teruyuki Yanagisawa and **Takeya Sato**.
第 12 回日本心不全学会学術集会、2008 年 10 月 16 日～10 月 18 日、東京

3) 抗ウィルス薬の副作用に関する分子薬理学研究
佐藤友香、助川 淳、柳澤輝行、**佐藤岳哉**
第 59 回日本薬理学会北部会、2008 年 9 月 27 日、仙台

4) ヒスタミン H3 受容体の細胞表面発現調節
木下和樹、高柳詩織、前田 恵、原口満也、**佐藤岳哉**、谷内一彦、福永浩司、柳澤輝行、助川 淳
第 59 回日本薬理学会北部会 2008 年 9 月 27 日、仙台

5) Apoptosis induction by the anti-retrovirus drug through mitochondrial dysfunction.
Yuka Sato, Jun Sukegawa, Teruyuki Yanagisawa, **Takeya Sato**.
XI Workshop on apoptosis in biology and medicine.2008 年 9 月 12 日～9 月 14 日、仙

台

6) 抗レトロウィルス薬代謝物のミトコンドリア機能に対する影響の評価
佐藤岳哉、助川淳、柳澤輝行
第 82 回日本薬理学会年会、2009 年 3 月 16 日～18 日、横浜

7) ヒスタミン H3 受容体の細胞表面発現調節
助川淳、木下和樹、高柳詩織、**佐藤岳哉**、前田恵、原口満也、谷内一彦、福永浩司、柳澤輝行
第 82 回日本薬理学会年会、2009 年 3 月 16 日～18 日、横浜

8) ヒスタミン H3 受容体に結合し発現量を制御するタンパク質の新たな同定
高柳詩織、木下和樹、**佐藤岳哉**、前田恵、原口満也、谷内一彦、福永浩司、柳澤輝行、助川淳
第 82 回日本薬理学会年会、2009 年 3 月 16 日～18 日、横浜

H. 知的財産権の出願・登録状況

1．特許取得

該当なし

2．実用新案登録

該当なし

3．その他

該当なし

別紙４

研究成果の刊行に関する一覧表

書籍

著者氏名	論文タイトル名	書籍全体の編集者名	書籍名	出版社名	出版地	出版年	ページ
該当なし							

雑誌

発表者名	論文タイトル名	発表誌名	巻号	ページ	出版年
Higuchi K, Ayach B, **Sato T**, Chen M, Devine SP, Rasaiah VI, Dawood F, Yanagisawa T, Tei C, Takenaka T, Liu PP, Medin JA.	Direct Injection of Kit Ligand-2 Lentivirus Improves Cardiac Repair and Rescues Mice Post-myocardial Infarction..	Mol. Ther.	17 (2)	262-268	2009.
Maeda K, Haraguchi M, Kuramasu A, **Sato T**, Ariake K, Sakagami H, Kondo H, Yanai K, Fukunaga K, Yanagisawa T, Sukegawa J.	CLIC4 interacts with histamine H3 receptor and enhances the receptor cell surface expression.	Biochem Biophys Res Commun.	369 (2)	603-608	2008.

別紙５
研究成果の刊行物・別刷

Direct Injection of Kit Ligand-2 Lentivirus Improves Cardiac Repair and Rescues Mice Post–myocardial Infarction

Koji Higuchi[1], Bilal Ayach[2–4], Takeya Sato[5], Manyin Chen[2], Sean P Devine[6], Vanessa I Rasaiah[1], Fayez Dawood[2], Teruyuki Yanagisawa[5], Chuwa Tei[7], Toshihiro Takenaka[8], Peter P Liu[2–4] and Jeffrey A Medin[1,2,4,6]

[1]*Division of Stem Cell and Developmental Biology, Ontario Cancer Institute, University Health Network, Toronto, Ontario, Canada;* [2]*Toronto General Research Institute, University Health Network, Toronto, Ontario, Canada;* [3]*The Heart and Stroke/Richard Lewar Centre of Excellence, University of Toronto, Toronto, Ontario, Canada;* [4]*Institute of Medical Sciences, University of Toronto, Toronto, Ontario, Canada;* [5]*Department of Molecular Pharmacology, Tohoku University Graduate School of Medicine, Sendai, Japan;* [6]*Department of Medical Biophysics, University of Toronto, Toronto, Ontario, Canada;* [7]*Department of Cardiovascular, Respiratory, and Metabolic Medicine, Graduate School of Medical and Dental Sciences, Kagoshima University, Kagoshima, Japan;* [8]*Division of Cardiac Repair and Regeneration, Graduate School of Medical and Dental Sciences, Kagoshima University, Kagoshima, Japan*

Myocardial infarction (MI) and subsequent adverse remodeling cause heart failure. Previously we demonstrated a role for Kit ligand (KL) in improving cardiac function post-MI. KL has two major isoforms; KL-1 is secreted whereas KL-2 is predominantly membrane bound. We demonstrate here first that KL-2-deficient mice have worse survival and an increased heart/bodyweight ratio post-MI compared to mice with reduced c-Kit receptor expression. Next we synthesized recombinant lentiviral vectors (LVs) that engineered functional expression of murine KL-1 and KL-2. For *in vivo* analyses, we directly injected these LVs into the left ventricle of membrane-bound KL-deficient *Sl/Sl*^{d} or wild-type (WT) mice undergoing MI. Control LV/enGFP injection led to measurable reporter gene expression in hearts. Injection of LV/KL-2 attenuated adverse left ventricular remodeling and dramatically improved survival post-MI in both *Sl/Sl*^{d} and WT mice (from 12 to 71% and 35 to 73%, respectively, versus controls). With regard toward beginning to understand the possible salutary mechanisms involved in this effect, differential staining patterns of Sca-1 and Ly49 on peripheral blood (PB) cells from therapeutically treated animals was found. Our data show that LV/KL-2 gene therapy is a promising treatment for MI.

Received 1 April 2008; accepted 10 June 2008; published online 11 November 2008. doi:10.1038/mt.2008.244

INTRODUCTION

Recent advances in understanding of the molecular mechanisms of cardiovascular disease, the role of stem cells in cardiac regeneration, and in gene delivery approaches allow thematic convergence for the development of novel treatments for heart disease. Although gene therapy has mainly been thought of as a treatment for cancer or inherited single-gene disorders, recent studies have shown that this therapeutic approach has the capability to treat multifactorial diseases, including myocardial infarction (MI).[1,2] Lentiviral vectors (LVs) are efficient gene delivery agents that have the capability to infect a variety of cell types including postmitotic cells. LVs have been approved for clinical utility and recent studies have demonstrated the use of these vectors in the treatment of cardiovascular disease.[3]

Adverse left ventricular remodeling post-MI triggers heart failure; it is important to prevent this outcome. Cytokine therapy post-MI is an attractive schema because such treatment might regenerate cardiac tissue and protect against adverse left ventricular remodeling.[4–6] For example, Woldbaek *et al.* have shown that mRNA expression of Kit ligand (KL or SCF), the ligand for the steel receptor tyrosine kinase (c-Kit) receptor, is decreased in the heart post-MI.[9] Furthermore, we have previously reported on detailed cardiac rescue and remodeling mechanisms post-MI involving the c-Kit receptor axis.[10]

KL has two isoforms, KL-1 and KL-2, which are formed by alternative splicing. KL-2 is missing a predominant extramembrane cleavage site[11] and is largely membrane bound. These two isoforms of KL have differential effects on the survival and proliferation of hematopoietic cells;[12,13] observations which are reinforced by the altered phenotype of *Sl/Sl*^{d} mice, which have only soluble KL. Importantly, membrane-associated KL has also demonstrated more potent and sustained signaling than its secreted counterpart.[14]

Recently, we reported α-galactosidase A correction in the hearts of animals in a Fabry disease model by direct intraventricular injection of a recombinant LV.[15] That study on an inherited disorder provided a conceptual platform for the broadening of this therapeutic schema to impact acquired disorders as well. The aims of this present study were to develop novel recombinant LVs that engineer expression of KLs and to investigate the effects of direct left ventricular injection of vectors post-MI in mice. Effective vectors were generated and functional KL expression was documented *in vitro*. Direct injection of a LV that engineered

Correspondence: *Jeffrey A. Medin, University Health Network, Room 406, 67 College Street, Toronto, Ontario, Canada. E-mail: jmedin@uhnres.utoronto.ca*

expression of enGFP led to appreciable functional transductions of cardiac tissue. Next we observed that the overexpression of KL-2 by direct cardiac injection prevents adverse remodeling and dramatically improves survival post-MI both in KL-2-deficient mice and in wild-type (WT) animals. Increased survival was also correlated with differential expression of cell surface antigens Ly49 and Sca-1 on peripheral blood (PB) cells. These results open the door to the development of this therapeutic modality for the treatment of cardiovascular disease.

RESULTS

Decreased survival and worsened cardiac function in *Sl/Sl*^{d} mice post-MI compared with *W/W*^{v} mice

Our previous studies have shown that null c-Kit mutation *w/w-viable* (*W/W*^{v}) mice have diminished heart function and greater cardiac dilatation than WT mice 35 days after MI.[10] We also demonstrated that these effects could be rescued by transplantation of WT bone marrow cells.[10] To focus our present studies on dissecting the contributions of individual components of the KL/c-Kit receptor axis, we first performed MIs on *W/W*^{v} and *Sl/Sl*^{d} mice. *Sl/Sl*^{d} mice produce only soluble KL.[11] **Figure 1** shows the results of preliminary studies providing survival percentages and heart/bodyweight ratio calculations measured at 5 weeks after MI. Clear differences were seen. *Sl/Sl*^{d} mice have markedly decreased survival percentages and an increased heart/bodyweight ratio in surviving animals at killing than *W/W*^{v} mice—indicating worsened outcomes post-MI.

KL overexpression in transduced Sl/Sl^{4} and TF-1 cells

Next, we developed novel LVs that engineer expression of KL-1 or KL-2 (LV/KL-1 and LV/KL-2, respectively). LV/KL-2 has an 84-bp deletion that removes the major proteolytic cleavage site; a minor cleavage site closer to the transmembrane domain is still maintained. LV/enGFP[16] was used as a control *in vitro*. VSV-g-pseudotyped LVs were generated and titered as before.[16] LVs were used to infect a KL-deficient murine stromal cell line, (Sl/Sl^{4} cells; ref. 17), at an MOI of 10. Nontransduced Sl/Sl^{4} cells were negative for KL expression while ~95% of infected cells expressed KL-1 and KL-2, respectively, as measured by flow cytometry analyses (**Figure 2a**). KL expression and protein relative molecular weights were confirmed by western blots performed on transduced Sl/Sl^{4} cell lysates (**Figure 2b**). Subsequently, the supernatant from pools of infected Sl/Sl^{4} cells was analyzed by ELISA to determine the concentration of cleaved KL (**Figure 2c**). As expected, more secreted KL-1 was observed in similarly infected cells because of the inclusion of the major cleavage site. Finally, the bioactivity of KL generated by LV/KL-1 or LV/KL-2 infection was verified by its ability to support the growth of a KL-dependent cell line, TF-1 (ref. 18). Here transduced TF-1 cell pools were shown to proliferate faster than nontransduced cell pools, indicating production of functional KL (data not shown).

LV-mediated enGFP expression in infarcted hearts

To evaluate marking transgene expression mediated by a single LV administration in compromised recipients, WT mice received an MI-generating ligation and then phosphate buffered saline (PBS) or LV/enGFP were directly injected into their hearts in a minimal volume. Mice were killed 7 days after the MI. As expected, the enGFP signal was detected in the LV/enGFP-treated hearts and not in the PBS-treated hearts (**Figure 3a,b**). To avoid misleading outcomes due to possible autofluorescence, immunostaining was also performed for enGFP with a monoclonal antibody and then these signals merged with the enGFP fluorescence signals (**Figure 3c–e**). Relative fluorescence intensity was also calculated from a number of mounts of whole tissue samples derived from animals injected with serial dilutions of LV/enGFP. **Figure 3f** demonstrates, as could be predicted, that increased amounts of LV/enGFP injected leads to increased fluorescence intensity in cardiac samples. Finally, we also determined the relative cellular transduction rate from a number of fields for each mouse tissue mount (**Figure 3g**). These data indicate that ~5% of cells were functionally transduced by this direct LV injection method. Combined with our previous data,[15] this indicates that this direct injection LV system is efficient for gene transfer into the heart.

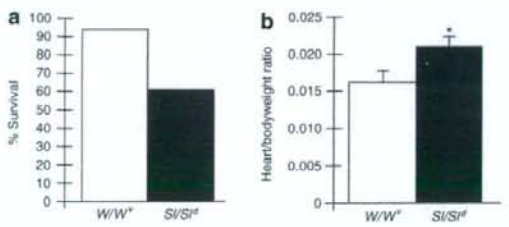

Figure 1 Comparison of functional outcomes in *W/W*^{v} mice (n = 10) and *Sl/Sl*^{d} mice (n = 10) that have undergone myocardial infarction (MI). (**a**) Percent survival measured at 5 weeks after MI. (**b**) Heart/bodyweight ratio of surviving animals measured at 5 weeks after MI. *P < 0.05.

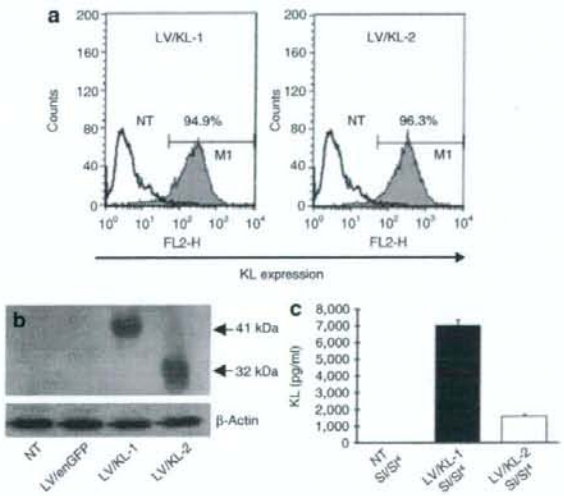

Figure 2 LV/KL-1 and LV/KL-2 efficiently infect Sl/Sl^{4} cells, a KL-deficient cell line. Transgene expression in infected cells was confirmed by (**a**) flow cytometry (KL expression in NT, LV/KL-1, and LV/KL-2 infected cells; 0.98%, 94.9%, and 96.3% respectively) and (**b**) western blot. For the western blot, LV/enGFP and nontransduced Sl/Sl^{4} cell extracts were used as controls. β-actin levels were evaluated as a protein loading control. (**c**) Cleaved KL in the supernatant of infected Sl/Sl^{4} cell pools was measured by ELISA. NT; nontransduced.

KL expression in the heart

To determine the effect of LV-mediated KL overexpression on recovery post-MI, our gene therapy strategy was tested in both *Sl/Sl*^{d} and in WT mice. These mice were randomized into six groups, receiving either MI or a sham operation. Within minutes after MI or sham operation, injection of the KL LVs was performed. Therapeutic transgene expression, mediated by direct vector injection, was then quantified. KL-2 expression was determined by ELISA from heart tissue of LV/KL-2-injected WT mice at 3 days after MI. KL-2 was observed to be overexpressed in the left ventricle of the LV/KL-2-injected hearts, including both the infarct and peri-infarct regions, compared to controls (**Figure 4a**). These results demonstrate that LV/KL-2 efficiently infects cardiac tissue from a single direct vector administration and generates KL-2 protein expression *in vivo*.

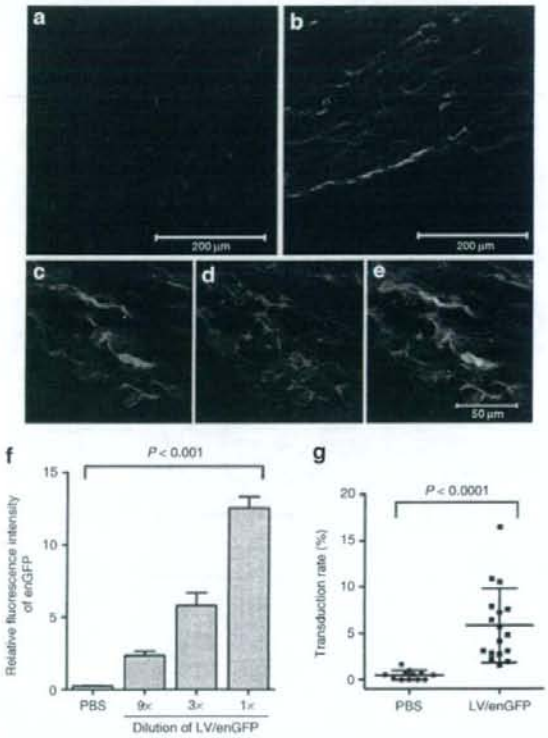

Figure 3 enGFP expression in the hearts of WT mice directly injected with LV/enGFP and receiving an MI. (**a**) PBS control–injected hearts and (**b**) LV/enGFP-injected hearts were examined for enGFP signal (green) and also stained with enGFP antibody (Alexa546, red). (**c**) enGFP signal at higher magnification. (**d**) Immunostaining for enGFP expression. (**e**) Overlay of **c** and **d** showing co-localization of the enGFP signal and enGFP staining. (**f**) Relative fluorescence intensity of the enGFP signal in hearts receiving direct injections of various doses of LV/enGFP. For each group 14 fields were analyzed per mouse injected ($n = 2$ or three animals per group). (**g**) Estimation of the transduction rate in cardiac tissue samples from LV/enGFP-injected mice. For the PBS-injected control group six fields were analyzed per mouse ($n = 2$ mice). For the LV-enGFP group 8 or 9 fields were analyzed per mouse ($n = 2$ mice).

LV/KL-2 administration substantially reduces infarct size and prevents adverse cardiac remodeling post-MI

Morphometric analysis was performed on injected WT mice at 7 and 35 days after MI. Representative results are shown in **Figure 4b**. In the LV/KL-2-treated group, left ventricular infarct sizes were significantly reduced (37.2 ± 2.5% versus 59.3 ± 3.0%, LV/KL-2 versus PBS respectively, $P < 0.001$) and left ventricular wall thickness was significantly improved at 35 days after MI (0.78 ± 0.24 mm versus 0.30 ± 0.03 mm, LV/KL-2 versus PBS respectively, $P < 0.05$) (**Figure 4c,d**).

Following cardiac remodeling post-MI, left ventricles are commonly dilated. In our study, we observed that the heart/bodyweight ratio in the LV/KL-2-treated group was significantly decreased compared with the PBS-treated group in WT mice ($0.0099 \pm 7.2 \times 10^{-4}$ versus $0.0123 \pm 6.8 \times 10^{-4}$, LV/KL-2 versus PBS respectively, $P < 0.05$) (**Figure 5a**). Furthermore, at 35 days after MI in WT mice, left ventricular end-diastolic volume and left ventricular end-systolic volume were reduced in LV/KL-1 and LV/KL-2-treated WT mice compared with PBS-treated WT mice (**Figure 5b,c**). These functional results show that LV/KL treatment prevented adverse cardiac remodeling in mice.

Direct LV/KL-2 injection markedly improves survival in *Sl/Sl*^{d} and WT mice post-MI

PBS-injected *Sl/Sl*^{d} mice demonstrated 12% survival at 35 days after MI (**Figure 6a**). In addition, animals receiving LV/KL-1 also had decreased survival frequencies (**Figure 6a**). In contrast,

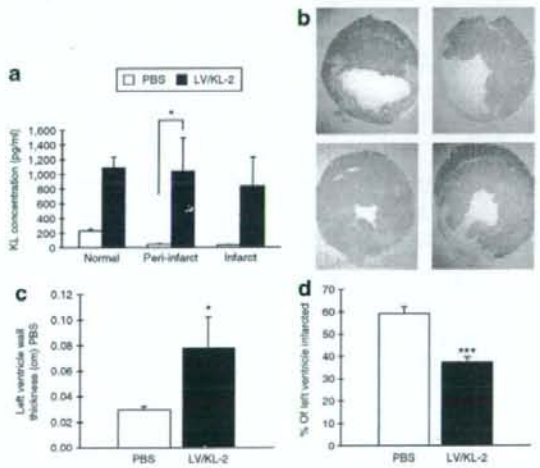

Figure 4 KL-2 expression in hearts and morphometric effects of LV/KL-2 gene therapy for MI. (**a**) Cardiac tissue KL expression as measured by ELISA at 3 days after MI in WT mice. Levels of KL are significantly greater in LV/KL-2-treated mice ($n = 3$) compared with PBS-treated mice ($n = 3$) in all areas of the heart. (**b**) Morphometrics (representative shown) demonstrate a smaller infarcted area in the left ventricle in LV/KL-2-treated WT mice compared with the PBS-treated group. (**c**) Left ventricular wall thickness and (**d**) the percent of left ventricle infarcted are significantly improved in LV/KL-2-treated WT mice ($n = 6$) at 35 days after MI compared with the PBS-treated group ($n = 6$). *$P < 0.05$, ***$P < 0.001$ compared with PBS-treated WT group.

survival was greatly improved in *Sl/Sl*^{d} mice treated with LV/KL-2, with 71% survival observed at 35 days ($P < 0.041$ versus PBS group) (**Figure 6a**). This result itself implicates the c-Kit receptor/KL axis as an important component of recovery post-MI and demonstrates that constructive manipulation of facets of that pathway can dramatically improve survival. Finally, we examined this therapeutic strategy in a more relevant model. We hypothesized that such robust repair mechanisms mediated by direct LV delivery of KL-2 could also work even in the context of existing normal recovery operations. Similar functional analyses were then performed in WT mice. Here we observed that survival of WT mice following MI was also significantly improved from 35 to 73.1% ($P < 0.05$) following LV/KL-2 treatment (**Figure 6b**).

Flow cytometric analyses of PB and immunohistochemistry from LV-injected and control mice post-MI

Toward gaining insights into mechanism, PB was obtained from surviving mice at days 0, 3, 7, 14, and 35 post-MI. MI is associated with a deleterious inflammatory response. Indeed, our previous results demonstrated that NK cells mediated cardiac survival and repair post-MI,[10] therefore mononuclear cells were analyzed for expression of a directed series of cell surface markers including Ly49 (NK and NK-T cells), CD11c (NK, monocytes, macrophages, subsets of T and B cells), CD94 (NK, NK-T, activated CD8+ T cells), CD117 (c-Kit), CD34 (endothelial cells and short-term reconstituting HSCs), and Sca-1 (HSCs, activated lymphocytes). Note that data from *Sl/Sl*^{d} mice receiving PBS post-MI could only be collected through 14 days because of high mortality. For some cell surface markers such as CD11c and CD34, values at day 35 were not different from starting values and were not dramatically impacted by the addition of LV/KL-2 (data not shown). This phenomenon also largely occurred with CD117 expression and CD94 expression (data not shown).

In contrast, for Ly49 expression starting values between the *Sl/Sl*^{d} and WT mice were quite similar (~5% of PB cells) as shown in **Figure 7a**. Yet at 14 days after MI these values started to diverge. Finally at 35 days both the *Sl/Sl*^{d} and WT mice receiving LV/KL-2 had significantly increased levels of Ly49^{+} cells in the PB (8.1 ± 2.4% and 6.8 ± 3.2%, respectively) in comparison with WT animals receiving PBS post-MI (2.5 ± 1.5%; $P < 0.006$) (**Figure 7a**).

Another class of responses were observed with the Sca-1 analyses. Concerning Sca-1, differences were seen in positive-staining percentages at baseline between WT and *Sl/Sl*^{d} animals at day 0 (~25% versus ~42%, respectively) (**Figure 7b**). These differences were largely maintained over the period of analysis. That is, except for those WT animals treated with the LV/KL-2. There at day 35, values for the WT animals treated with LV/KL-2 were dramatically different than those from animals treated with PBS only following MI (39.2 ± 13.5% positive versus 20.2 ± 11.0% positive, respectively; $P < 0.034$). Further subset analysis of this group, *i.e.*, co-staining for Sca-1 and CD34 jointly, did not reveal differences in the numbers of cells dually positive for those markers, however (data not shown).

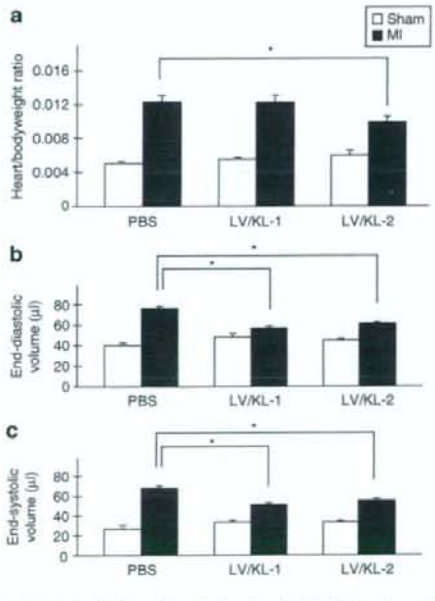

Figure 5 Physiological profiles following LV/KL-2 treatment for MI. LV/KL-2-treated WT mice ($n = 8$) demonstrate marked improvement in (**a**) Heart/bodyweight ratio, (**b**) left ventricular end-diastolic volume (LVEDP), and (c) left ventricular end-systolic volume (LVESV) compared with the PBS-treated group ($n = 3$). *$P < 0.05$, ***$P < 0.001$.

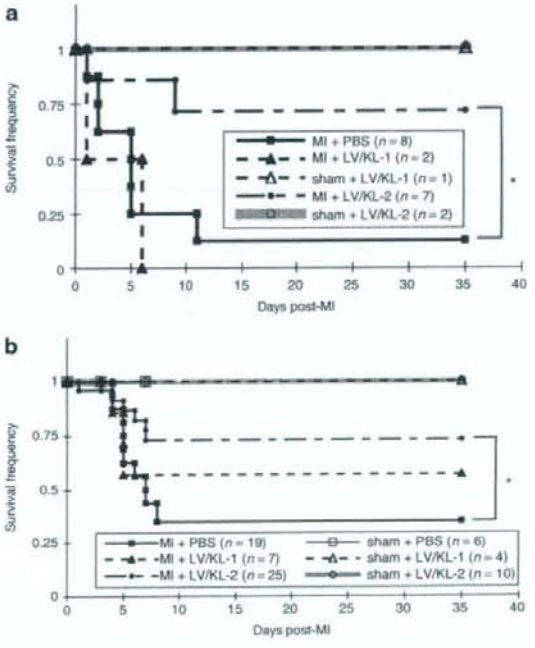

Figure 6 Direct LV/KL-2 injection enhances survival post-MI. LV/KL-2-treated (**a**) *Sl/Sl*^{d} and (**b**) WT mice demonstrate dramatically improved survival post-MI compared with PBS-treated mice. *$P < 0.05$, ***$P < 0.02$.

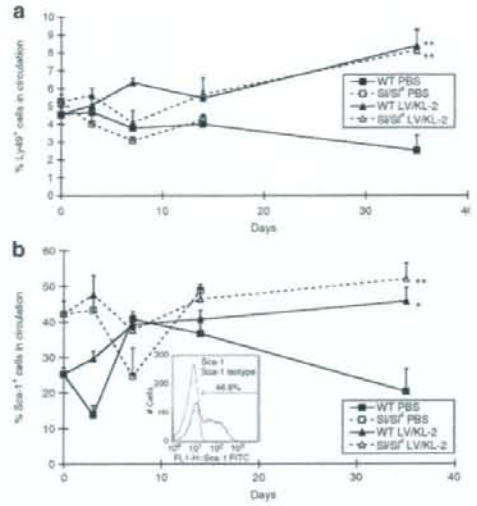

Figure 7 Results of flow cytometric analyses for Ly49 and Sca-1 staining of peripheral blood from WT and *Sl/Sl*^{d} mice treated with PBS or LV/KL-2 following MI. (**a**) Ly49^{+} cell mobilization over 35 days. (**b**) Sca-1^{+} cell mobilization over 35 days. Inset: Sample flow cytometry analysis for Sca-1 staining with isotype control. $^{*}P < 0.05$, $^{**}P < 0.01$.

DISCUSSION

We have demonstrated that the LV gene delivery system is a promising approach for the treatment of MI; especially when the KL/c-Kit signaling axis (specifically KL-2) is accessed. LVs are able to transduce nondividing cells[19] such as cardiomyocytes, integrate into the genome, and provide long-term transgene expression.[20] Indeed, Fleury *et al.* have shown efficient LV transduction and transgene expression *in vitro* in adult rat cardiomyocytes.[21] Lower levels of sustained expression of KL-2 as generated by LV-mediated delivery may provide more benefit over time as repair is an ongoing process, compared to the higher bolus amounts of cytokines that would be produced using other transient delivery systems such as recombinant adenoviruses, for example. Outcomes from experiments designed to test this hypothesis would be interesting and provide further insights into mechanisms and timing of cardiac repair.

Our *in vitro* results demonstrate generation of effective recombinant LVs that drive expression of KLs. Our *in vivo* results demonstrate that LV-mediated KL-2 overexpression mediated by a single gene delivery event targeted directly into the murine myocardium dramatically improves hemodynamics and morphometrics (Figures 4 and 5, respectively) as well as survival of both KL-2-deficient and even WT mice post-MI (**Figure 6**). Indeed the robustness of this response is striking in the WT group given that normal signaling and repair pathways are still present in these animals. These results imply that membrane-bound KL is an important molecule in recovery and in prevention of adverse cardiac remodeling post-MI. These findings thus extend into the therapeutic realm results from our previous studies demonstrating the importance of systemic KL and c-Kit signaling in remodeling and rescue of the infarcted heart.[10] Note that we have also performed studies with imatinib mesylate (Gleevec), which is a pleiotropic agent that also blocks c-Kit function, and found a significant increase in animal mortality after MI over untreated animals (data not shown).

The mechanism whereby cytokine therapy prevents adverse cardiac remodeling has yet to be fully elucidated. It has been proposed that bone marrow cells are homing to the infarcted heart and transdifferentiate into cardiomyocytes post-MI.[5,22,23] These cells may play an important role in cardiac remodeling post-MI. Recently, Dawn *et al.* have suggested that mobilization of cardiac stem cells themselves by cytokines could be an additional or alternative mechanism.[8,24] Along these lines, it bears mentioning that we observed improved survival with LV/KL-2 compared to animals treated with LV/KL-1 (**Figure 6a**), although many fewer animals were tested in the second case. This may indicate a more pronounced requirement for the membrane-bound form of KL in cardiac rescue and remodeling post-MI, perhaps acting through an autocrine manner. These results may delineate a novel function for this isoform. On the other hand, we also show in **Figure 2** that some detectable KL is secreted even from the form missing the major cleavage site. Thus perhaps both autocrine and paracrine mechanisms are at play here. In support of this hypothesis we see alterations in the nature of circulatory PB cells in treated animals (**Figure 7**). One difference between the two forms is in the duration and intensity of signaling, which is increased with KL-2 (ref. 14). KL-1 and KL-2 may also thus stimulate different homing or remodeling signals in this context.

For clinical application, further experiments need to be performed in order to address any pertinent safety concerns—such as any side effects with sustained overexpression of KL—and the optimal timing of vector administration following MI. Transcriptionally targeted vectors exploiting cardiac-specific promoters[25,26] built into the next generation of recombinant LVs constructed for this purpose, for example, would decrease the likelihood of possible off-target expression effects. Likewise, the tropism of the vector may be made more restricted or the delivery system itself may be modified to further increase the potency of this approach. Concerning the timing of vector administration, these present proof-of-principle studies were undertaken wherein the MI and the vector delivery were performed immediately sequentially to address technical concerns and Animal Care Committee issues. Future studies, perhaps in rats (or other larger animal models) to relieve these concerns and optimize the timing of LV/KL-2 delivery to maximize beneficial outcomes following MI in the context of real world timing will be undertaken.

In summary, this is the first study to show improvement in survival using a novel direct LV gene therapy strategy and provides the platform for further development of this approach for potential treatment of MI.

MATERIALS AND METHODS

LVs. HIV-1 based recombinant LVs were constructed by replacing the enhanced GFP (enGFP) in pHR'-cPPT-EF-GW-SIN plasmid with the KL-1 or KL-2 cDNAs (LV/KL-1 or LV/KL-2). This construction method was previously described.[16] The KL-1 cDNA was subcloned out from C57Bl/6 mice. Briefly, total RNA was isolated from stroma cells using the TRIzol reagent (Invitrogen, Carlsbad, CA). First strand cDNA was synthesized from 1 μg total RNA using the SuperScript First Strand Synthesis System (Invitrogen). The specific KL-1 cDNA was amplified by PCR using primers

based on the published mouse KL-1 mRNA sequence (NM_013598). Forward primer: 5′-CGCTGCCTTTCCTTATGAAG-3′ and Reverse primer: 5′-CGTCCACAATTACACCTCTTG-3′. KL-1 amplicons of ~850 bp were obtained after amplification for 35 cycles (denaturing at 94 °C, 45 seconds; annealing at 57 °C, 45 seconds; elongation at 72 °C, 60 seconds) using Platinum Taq DNA polymerase High Fidelity reagents (Invitrogen). The mouse KL-1 cDNA product was subcloned using the PCR-Script Amp cloning Kit (Stratagene, La Jolla, CA).

KL-2 lacks the codon for exon 6 of the KL-1 sequence. To remove exon 6 from the KL-1 cDNA, inverse PCR was performed on the pPCR-Script/KL-1 plasmid template. The forward primer targeted the 3′ end of exon 5 of the KL-1 cDNA and the reverse primer targeted the 5′ end of exon 7 of KL-1 cDNA. Forward primer; 5′-CTTTCTCGGGACCTAATGTTG-3′; Reverse primer; 5′-GGAAAGCCGCAAAGGCCC-3′. Inverse PCR was performed using Platinum Taq DNA polymerase High Fidelity reagents for 35 cycles. Each cycle consisted of the following steps: denaturation at 94 °C, 30 seconds; annealing at 54 °C, 5 minutes; extension at 68 °C, 5 minutes each. The inverse PCR product was then self-ligated to make plasmid, which contains the KL-2 cDNA. This product (pPCR-Script/KL-2) was transformed into XL10-Gold Ultracompetent cells (Stratagene) and verified by DNA sequencing.

Vesicular stomatitis virus glycoprotein-pseudotyped (VSV-g) LVs, including an enGFP control vector (LV/enGFP) used *in vitro*, were generated by transient transfection of 293T cells (obtained form Michele Calos, Stanford University) using the three-plasmid system (LV plasmid construct, packaging plasmid pCMVΔR8.91, and the VSV-g envelope-coding plasmid pMD.G) with FuGENE6 (Roche, Indianapolis, IN). Virus supernatant were harvested at 48 hours and concentrated at 50,000*g* for 2 hours. The concentrated viral supernatants were serially diluted and titered on 293T cells. p24 antigen levels also were determined by an HIV-1 p24 ELISA (PerkinElmer, Waltham, MA).

Functional expression of KL transgenes in the Sl/SL4 and TF-1 cell lines. The Sl/Sl^4 cell line was purchased from ATCC (Manassas, VA). Sl/Sl^4 cells were cultured in Dulbecco's Modified Eagle Medium with 10% fetal bovine serum, 100 IU of penicillin/ml and 100 μg of streptomycin/ml. A half million Sl/Sl^4 cells were infected a single time with LV/KL-1, LV/KL-2, or LV/enGFP at an MOI of 10 in the presence of 8 μg/ml protamine sulfate. Flow cytometric analyses were performed 2 days later. Transduced Sl/Sl^4 cells were also lysed in sample buffer and cell lysates were resolved by SDS-PAGE and transferred onto polyvinylidene difluoride filters (Millipore, Billerica, MA). Filters were blocked with 10% skim milk in PBS with 0.1% Tween20 for 1 hour at RT. KL was detected with biotinylated anti-mouse KL antibody (BAF455; R&D Systems, Minneapolis, MN), used at 0.2 μg/ml. Equal protein loading was confirmed with an anti-β-actin antibody (A5441; Sigma Aldrich, St Louis, MO) diluted 1:10,000. Blots were probed with secondary anti-goat (diluted 1:5,000, sc-2020; Santa Cruz Biotechnology, Santa Cruz, CA) or anti-mouse (diluted 1:1,000, NA931; GE Healthcare, Piscataway, NJ) horseradish peroxidase–conjugated antibodies. Protein bands were detected using an enhanced Chemiluminesence kit (Perkin Elmer, Waltham, MA).

Transduced or nontransduced Sl/Sl^4 cells were seeded in a 10-cm dish in 10 ml of DMEM with 10% fetal bovine serum. Supernatant was harvested 2 days later and KL concentration was measured using the SCF ELISA kit (R&D Systems).

TF-1 cells, which are a human erythroblast cell line, were obtained from ATCC. TF-1 cells were infected with LV/KL-1 and LV/KL-2 at an MOI of 5. Three days after transduction, infected TF-1 cells were harvested and the cells were washed with PBS twice. TF-1 cells were incubated with biotinylated anti-mouse SCF antibody (R&D Systems) at 4 °C for 20 minutes and washed twice with PBS. These cells were incubated with streptavidin-phycoerythrin (BD Biosciences, San Jose, CA) at 4 °C for 20 minutes and washed with PBS twice. Expression of KL-1 and KL-2 on infected TF-1 cells was determined by flow cytometry and found to be 68.9 and 49.2 %, respectively (data not shown).

Experimental animals. WBB6F1/J-Kit^W/Kit^{W-v} (*W/W^v*) mice, WCB6F1/J *Kitl^{Sl} kitl^{Sl-d}* (*Sl/Sl^d*) mice, and their littermates (WT) were purchased from the Jackson Laboratory (Bar Harbor, ME). Animal experiments were performed under protocols approved by the University Health Network Animal Care Committee.

Induction of MI and cardiac injection of LVs. MI was induced by permanent ligation of the left anterior descending coronary artery as described previously.[27] Forty microliters of LVs (corresponding to 2.8 μg/ml p24 antigen) or PBS were injected into the left ventricle as before.[13]

In vivo *study plan.* In experiment 1, *Sl/Sl^d* ($n = 20$) and WT ($n = 37$) mice were randomized into six groups. Mice received either an MI or sham operation and then PBS or LVs encoding KL-1 or KL-2 were injected directly into the left ventricle. Mice were monitored for morbidity and mortality. The percentages of death from the MI/injection procedure itself and controls, in *Sl/Sl^d*+MI, *Sl/Sl^d*+sham, WT+MI, and WT+sham groups, were 52.9, 50, 10.5, and 4.8%, respectively. At 35 days after MI, mice were killed after the evaluation of cardiac function. In experiment 2, WT mice ($n = 34$) were subjected to MI or sham operation and PBS or LV/KL-2 were injected. Some mice were randomly killed for analyses on 3, 7, and 35 days after MI.

In experiment 3, to check the efficiency of LV-mediated gene transfer into the heart, WT mice received an MI operation and were injected with PBS or LV/enGFP ($n = 3$ for each group) and were killed for immunohistochemistry 7 days after MI.

Flow cytometric analyses and antigen retrieval staining. PB was collected at 0, 3, 7, 14, and 35 days after MI. Cell surface expression of marker proteins on PB cells were analyzed by flow cytometry. Twenty microliters of PB cells were lysed with Red Blood Cell Lysing Buffer (Sigma) and incubated with antibody against Ly49, CD11c, CD94, CD117, Sca-1, and CD34 (all antibodies were purchased from BD Biosciences). PB cells were analyzed on a FACSCalibur flow cytometer (BD, Franklin Lakes, NJ).

To perform antigen retrieval staining for enGFP, heart sections were incubated in HistoVT One (Nacalai Tesque, Kyoto, Japan) for 20 minutes at 70 °C. The tissues were permeablized with PBS-T (0.1% Triton X-100 in PBS). The sections were incubated with anti-GFP monoclonal antibody (Nacalai Tesque, clone GF090R), and subsequently incubated with Alexa546-labeled goat anti-rat IgG antibody (Molecular Probes, Eugene, OR).

Cardiac function and morphometric evaluation. Cardiac function was analyzed using a Millar pressure volume conductance catheter. Morphometrics were analyzed as described before.[27] Briefly, hearts were harvested, rinsed with PBS, and embedded in OCT. Tissue was sectioned at 5 μm and stored at −80 °C until analysis. Digitally captured pathological images were used to evaluate the left ventricular area, wall thickness, and percent-infarcted area.

Statistical analyses. All statistical analyses were performed using a two-sample Student's *t*-test assuming unequal variance. For Kaplan–Meier curves, a logrank test was used to evaluate significance.

ACKNOWLEDGMENTS

This work was supported, in part, by the Heart and Stroke Foundation of Ontario and the Canadian Institutes of Health Research. We thank Makoto Yoshimitsu (Kagoshima University) for invaluable assistance.

REFERENCES

1. Sasano, T, McDonald, AD, Kikuchi, K and Donahue, JK (2006). Molecular ablation of ventricular tachycardia after myocardial infarction. *Nat Med* **12**: 1256–1258.
2. Kusano, KF, Pola, R, Murayama, T, Curry, C, Kawamoto, A, Iwakura, A *et al.* (2005). Sonic hedgehog myocardial gene therapy: tissue repair through transient reconstitution of embryonic signaling. *Nat Med* **11**: 1197–1204.

3. Higuchi, K and Medin, JA (2007). Lentiviral vectors for gene therapy of heart disease. *J Cardiol* **49**: 1–11.
4. Takahashi, T, Kalka, C, Masuda, H, Chen, D, Silver, M, Kearney, M *et al.* (1999). Ischemia- and cytokine-induced mobilization of bone marrow-derived endothelial progenitor cells for neovascularization. *Nat Med* **5**: 434–438.
5. Orlic, D, Kajstura, J, Chimenti, S, Limana, F, Jakoniuk, I, Quaini, F *et al.* (2001). Mobilized bone marrow cells repair the infarcted heart, improving function and survival. *Proc Natl Acad Sci USA* **98**: 10344–10349.
6. Kawada, H, Fujita, J, Kinjo, K, Matsuzaki, Y, Tsuma, M, Miyatake, H *et al.* (2004). Nonhematopoietic mesenchymal stem cells can be mobilized and differentiate into cardiomyocytes after myocardial infarction. *Blood* **104**: 3581–3587.
7. Harada, M, Qin, Y, Takano, H, Minamino, T, Zou, Y, Toko, H *et al.* (2005). G-CSF prevents cardiac remodeling after myocardial infarction by activating the Jak-Stat pathway in cardiomyocytes. *Nat Med* **11**: 305–311.
8. Dawn, B, Guo, Y, Rezazadeh, A, Huang, Y, Stein, AB, Hunt, G *et al.* (2006). Postinfarct cytokine therapy regenerates cardiac tissue and improves left ventricular function. *Circ Res* **98**: 1098–1105.
9. Woldbaek, PR, Hoen, IB, Christensen, G and Tonnessen, T (2002). Gene expression of colony-stimulating factors and stem cell factor after myocardial infarction in the mouse. *Acta Physiol Scand* **175**: 173–181.
10. Ayach, BB, Yoshimitsu, M, Dawood, F, Sun, M, Arab, S, Chen, M *et al.* (2006). Stem cell factor receptor induces progenitor and natural killer cell-mediated cardiac survival and repair after myocardial infarction. *Proc Natl Acad Sci USA* **103**: 2304–2309.
11. Ashman, LK (1999). The biology of stem cell factor and its receptor C-kit. *Int J Biochem Cell Biol* **31**: 1037–1051.
12. Miyazawa, K, Williams, DA, Gotoh, A, Nishimaki, J, Broxmeyer, HE and Toyama, K (1995). Membrane-bound Steel factor induces more persistent tyrosine kinase activation and longer life span of c-kit gene-encoded protein than its soluble form. *Blood* **85**: 641–649.
13. Caruana, G, Ashman, LK, Fujita, J and Gonda, TJ (1993). Responses of the murine myeloid cell line FDC-P1 to soluble and membrane-bound forms of steel factor (SLF). *Exp Hematol* **21**: 761–768.
14. Caruana, G, Cambareri, AC and Ashman, LK (1999). Isoforms of c-KIT differ in activation of signaling pathways and transformation of NIH3T3 fibroblasts. *Oncogene* **18**: 5573–5581.
15. Yoshimitsu, M, Higuchi, K, Dawood, F, Rasaiah, VI, Ayach, B, Chen, M *et al.* (2006). Correction of cardiac abnormalities in fabry mice by direct intraventricular injection of a recombinant lentiviral vector that engineers expression of alpha-galactosidase A. *Circ J* **70**: 1503–1508.
16. Yoshimitsu, M, Sato, T, Tao, K, Walia, JS, Rasaiah, VI, Sleep, GT *et al.* (2004). Bioluminescent imaging of a marking transgene and correction of Fabry mice by neonatal injection of recombinant lentiviral vectors. *Proc Natl Acad Sci USA* **101**: 16909–16914.
17. Toksoz, D, Zsebo, KM, Smith, KA, Hu, S, Brankow, D, Suggs, SV *et al.* (1992). Support of human hematopoiesis in long-term bone marrow cultures by murine stromal cells selectively expressing the membrane-bound and secreted forms of the human homolog of the steel gene product, stem cell factor. *Proc Natl Acad Sci USA* **89**: 7350–7354.
18. Kitamura, T, Tange, T, Terasawa, T, Chiba, S, Kuwaki, T, Miyagawa, K *et al.* (1989). Establishment and characterization of a unique human cell line that proliferates dependently on GM-CSF, IL-3, or erythropoietin. *J Cell Physiol* **140**: 323–334.
19. Naldini, L, Blomer, U, Gallay, P, Ory, D, Mulligan, R, Gage, FH *et al.* (1996). In vivo gene delivery and stable transduction of nondividing cells by a lentiviral vector. *Science* **272**: 263–267.
20. Naldini, L, Blomer, U, Gage, FH, Trono, D and Verma, IM (1996). Efficient transfer, integration, and sustained long-term expression of the transgene in adult rat brains injected with a lentiviral vector. *Proc Natl Acad Sci USA* **93**: 11382–11388.
21. Fleury, S, Simeoni, E, Zuppinger, C, Deglon, N, von Segesser, LK and Kappenberger, L *et al.* (2003). Multiply attenuated, self-inactivating lentiviral vectors efficiently deliver and express genes for extended periods of time in adult rat cardiomyocytes *in vivo*. *Circulation* **107**: 2375–2382.
22. Orlic, D, Kajstura, J, Chimenti, S, Jakoniuk, I, Anderson, SM, Li, B *et al.* (2001). Bone marrow cells regenerate infarcted myocardium. *Nature* **410**: 701–705.
23. Jackson, KA, Majka, SM, Wang, H, Pocius, J, Hartley, CJ, Majesky, MW *et al.* (2001). Regeneration of ischemic cardiac muscle and vascular endothelium by adult stem cells. *J Clin Invest* **107**: 1395–1402.
24. Linke, A, Muller, P, Nurzynska, D, Casarsa, C, Torella, D, Nascimbene, A *et al.* (2005). Stem cells in the dog heart are self-renewing, clonogenic, and multipotent and regenerate infarcted myocardium, improving cardiac function. *Proc Natl Acad Sci USA* **102**: 8966–8971.
25. Wang, Q, Sigmund, CD and Lin, JJ-C (2000). Identification of *cis* elements in the cardiac troponin T gene conferring specific expression in cardiac muscle of transgenic mice. *Circ Res* **86**: 478–484.
26. Su, H, Joho, S, Huang, Y, Barcena, A, Arakawa-Hoyt, J, Grossman, W *et al.* (2004). Adeno-associated viral vector delivers cardiac-specific and hypoxia-inducible VEGF expression in ischemic mouse hearts. *Proc Natl Acad Sci USA* **101**: 16280–16285.
27. Sun, M, Dawood, F, Wen, WH, Chen, M, Dixon, I, Kirshenbaum, LA *et al.* (2004). Excessive tumor necrosis factor activation after infarction contributes to susceptibility of myocardial rupture and left ventricular dysfunction. *Circulation* **110**: 3221–3228.

Available online at www.sciencedirect.com
ScienceDirect
Biochemical and Biophysical Research Communications 369 (2008) 603–608
BBRC
www.elsevier.com/locate/ybbrc

CLIC4 interacts with histamine H3 receptor and enhances the receptor cell surface expression

Kay Maeda [a,b,1], Mitsuya Haraguchi [a,c,1], Atsuo Kuramasu [d], Takeya Sato [a,b], Kyohei Ariake [e], Hiroyuki Sakagami [f], Hisatake Kondo [g], Kazuhiko Yanai [d], Kohji Fukunaga [b,c], Teruyuki Yanagisawa [a,b], Jun Sukegawa [a,b,*]

[a] *Department of Molecular Pharmacology, Tohoku University Graduate School of Medicine, Sendai 980-8575, Japan*
[b] *Tohoku University 21st Century COE Program "CRESCENDO", Sendai 980-8575, Japan*
[c] *Department of Pharmacology, Graduate School of Pharmaceutical Sciences, Tohoku University, Sendai 980-8578, Japan*
[d] *Department of Pharmacology, Tohoku University Graduate School of Medicine, Sendai 980-8575, Japan*
[e] *Department of Gastroenterological Surgery, Tohoku University Graduate School of Medicine, Sendai 980-8575, Japan*
[f] *Department of Anatomy, Kitasato University School of Medicine, Sagamihara 228-8555, Japan*
[g] *Department of Cell Biology, Tohoku University Graduate School of Medicine, Sendai 980-8575, Japan*

Received 12 February 2008
Available online 25 February 2008

Abstract

Histamine H3 receptor (H3R), one of G protein-coupled receptors (GPCRs), has been known to regulate neurotransmitter release negatively in central and peripheral nervous systems. Recently, a variety of intracellular proteins have been identified to interact with carboxy (C)-termini of GPCRs, and control their intracellular trafficking and signal transduction efficiencies. Screening for such proteins that interact with the C-terminus of H3R resulted in identification of one of the chloride intracellular channel (CLIC) proteins, CLIC4. The association of CLIC4 with H3R was confirmed in *in vitro* pull-down assays, coimmunoprecipitation from rat brain lysate, and immunofluorescence microscopy of rat cerebellar neurons. The data from flowcytometric analysis, radioligand receptor binding assay, and cell-based ELISA indicated that CLIC4 enhanced cell surface expression of wild-type H3R, but not a mutant form of the receptor that failed to interact with CLIC4. These results indicate that, by binding to the C-terminus of H3R, CLIC4 plays a critical role in regulation of the receptor cell surface expression.

Keywords: G protein-coupled receptor; Histamine H3 receptor; CLIC4; Trafficking

Histamine regulates numerous functions of central and peripheral nervous systems, including sleep-wake cycle, arousal, cognition, memory, and pain processing, through four receptor subtypes: H1, H2, H3 and H4 [1]. H3R has been known to inhibit synaptic release of a variety of neurotransmitters including histamine, acetylcholine, dopamine, noradrenaline, glutamate, γ-aminobutyric acid (GABA) [2]. Accordingly, H3R has attracted considerable interest from many pharmaceutical companies as a potential drug target for treatment of various pathological states including neuropathic pain and Alzheimer's disease [1].

In recent years, a growing number of cellular molecules have been identified to interact with C-terminal cytoplasmic domain of GPCR, and in most cases these interactions have been implicated in targeting, intracellular trafficking and subsequent signaling of GPCR [3]. Our previous work also showed that cell surface expression of PTH/PTH-

Abbreviations: CLIC4, chloride intracellular channel 4; ELISA, enzyme-linked immunosorbent assay; GPCR, G protein-coupled receptor; GST, glutathione-*S*-transferase; H3R, histamine H3 receptor; MBP, maltose binding protein.

* Corresponding author. Address: Department of Molecular Pharmacology, Tohoku University Graduate School of Medicine, Sendai 980-8575, Japan. Fax: +81 22 717 8065.
E-mail address: jsukegaw@mail.tains.tohoku.ac.jp (J. Sukegawa).
[1] These authors contributed equally to this work.

0006-291X/$ - see front matter © 2008 Elsevier Inc. All rights reserved.
doi:10.1016/j.bbrc.2008.02.071

related protein receptor is regulated by interaction of its C-terminal domain with some cellular molecule [4]. With the advancement of the research, it is now becoming increasingly clear that intracellular trafficking and subcellular localization of GPCRs are regulated in elaborate detail through these interactions [5].

CLIC4 belongs to CLIC protein family that consists of seven highly homologous proteins: CLIC1-4, 5A, 5B (p64), and 6 (parchorin). These proteins are widely expressed in multicellular organisms and implicated in anion transport within various subcellular compartments. Among them, however, only CLIC1, CLIC4, and CLIC5 have been shown directly to display anion channel activities in reconstituted planar lipid bilayer systems, albeit with poor selectivity [6]. CLIC proteins share a core structural domain of approximate 240 amino acid residues with a single transmembrane domain. A crystal structure study on CLIC4 revealed that the core domain of this protein family has a feature as the omega class glutathione-*S*-transferase proteins, and pointed to the structural foundation of the ability of this domain to conformationally transform itself from a soluble globular protein to an integral membrane protein [7]: an unusual feature shared among CLIC family proteins to "autoinsert" themselves into membranes [8]. CLIC4 has been reported to locate in membrane systems including endoplasmic reticulum (ER), caveola and *trans*-Golgi network, mitochondrial inner membrane, dense core secretary vesicles, and plasma membrane [8]. A study on the CLIC-related protein EXC-4 in *Caenorhabditis elegans* indicated that the protein is indispensable for lumen formation of excretory tube of the nematode [9]. It is also reported that CLIC4 is essential for tubular morphogenesis of cultured human endothelial cells [10]. While other reports suggest that CLIC4 associates with a variety of cellular proteins including dynamin I, 14-3-3 proteins, and rhodopsin [11,12], biological roles of these interactions are largely unknown.

Adding to the reported functional diversity, we present here a new observation that CLIC4 exerts a critical influence on H3R cell surface expression through binding to the C-terminal cytoplasmic domain of the receptor.

Materials and methods

Cell culture. CHO and PC12 cells were grown in DMEM supplemented with 10% FCS, and with 10% horse serum and 5% FCS, respectively. These cells were obtained from Cell Resource Center for Biomedical Research, Tohoku University (Sendai, Japan).

Yeast two-hybrid screening. The screening was carried out using the ProQuest Two-Hybrid System (Invitrogen, CA, USA) according to the manufacturer's recommendation.

In vitro pull-down experiment. The plasmid encoding GST-fused H3R (amino acids 414–445) was constructed from pGEX-5X-2 plasmid (GE Healthcare, UK). The coding sequence for CLIC4 (amino acids 56–253) obtained in the screening was inserted into pMAL-c2 vector (New England BioLabs, MA, USA) to generate MBP-CLIC4 fusion protein. The point mutations of H3R were generated with the aid of QuickChange site-directed mutagenesis kit (Stratagene, CA, USA). Cleared lysates of *Escherichia coli* containing GST-H3R or MBP-CLIC4 fusion protein were mixed and incubated for 1 h. After further incubated with glutathione-Sepharose 4B (GE Healthcare) for 1 h, proteins associated with the beads were separated on SDS–PAGE and probed with anti-MBP antibody (Cell Signaling Technology, MA, USA). Signals were visualized by HRP-conjugated secondary antibody and ImmunStar HRP substrate (Bio-Rad Laboratories, CA, USA).

Antibody production and immunoprecipitation. A recombinant CLIC4 protein (amino acids 56–253) was used to raise mouse anti-CLIC4 antibody. The antibody was affinity purified by using MicroLink protein coupling gel (Pierce, IL, USA). For production of H3R specific antibody, rabbits were immunized with GST-fused N-terminal domain of H3R (amino acids 1–30), and affinity purified by using MBP-H3R(1–30). Immunoprecipitation was performed as described [13].

Generation of recombinant adenoviruses. The recombinant adenoviruses (rAd-CLIC4, rAd-H3R, rAd-H3RF419A, and rAd-βgal) were generated from pAxCAwtit cosmid vector (Nippon Gene, Japan) according to manufacturer's recommendation. In all experiments, total number of viruses was adjusted by adding rAd-βgal expressing β-galactosidase.

Primary culture. Cerebella of E17 Wistar rat embryos were dissected according to protocols provided by Sumitomo Bakelite Co., Ltd. (Tokyo, Japan). Cerebellar cells cultured on poly-D-lysine/laminin-coated coverslips were subjected to immunofluorescence analysis on 22 days *in vitro*. All experimental procedures were complied with the Animals (Scientific Procedures) Act 1986 and the guidelines of the Ministry of Health, Labour and Welfare of Japan, and approved by Institute for Animal Experimentation Tohoku University Graduate School of Medicine.

Immunofluorescence microscopy. PC12 cells plated on coverslips precoated with collagen type IV were coinfected with rAd-H3R (MOI = 2) and rAd-CLIC4 (MOI = 100). Forty-eight hours after infection, cells were fixed in phosphate buffered saline (PBS) containing 4% paraformaldehyde (PFA). After blocking in PBS containing 20% normal goat serum, the cells were incubated with anti-H3R antibody. To locate intracellular CLIC4, cells were permeabilized with 0.1% Triton X-100 in PBS, and incubated with anti-CLIC4 antibody. Cells were then incubated with Alexa Fluor 546-conjugated anti-rabbit and Alexa Fluor 488-conjugated anti-mouse antibodies (Invitrogen), and inspected by Digital Eclipse C1 confocal microscope (Nikon, Japan). Cerebellar cells were fixed in 4% PFA in PBS, and then in cold methanol. Cells were permeabilized with 0.2% Triton X-100 in PBS, and blocked in 1% blocking reagent (TSA kit, Invitrogen). Blocked cells were incubated with anti-H3R and anti-CLIC4 antibodies, and then with Alexa Fluor 546-conjugated anti-rabbit antibody, HRP-conjugated anti-mouse antibody (Cell Signaling Technology), Alexa Fluor 488 tyramide (TSA kit), and Alexa Fluor 647-conjugated anti-calbindin D-28K antibody.

Flow cytometry. Cell surface H3R of PC12 cells coinfected with rAd-H3R (MOI = 2) and rAd-CLIC4 was labeled with anti-H3R antibody, followed by Alexa Fluor 488-conjugated anti-rabbit antibody. Cell-associated fluorescence was detected by a BD FACSCalibur flow cytometer (BD Biosciences, CA, USA). To measure whole cell H3R expression, the cells were permeabilized with 0.1% Triton X-100 in PBS. All data were analyzed with CellQuest software (BD Biosciences).

Radioligand receptor binding assay. PC12 cells infected with rAd-H3R (MOI = 2) and rAd-CLIC4 were incubated for 1 h in binding buffer (50 mM Tris–HCl, pH 7.4, and 5 mM EDTA) with 2 nM [^{3}H]-(R)-(−)-α-methylhistamine ([^{3}H]-RaMH), a selective H3R agonist. After the cells were separated and washed on glass fiber filters, the cell-associated radioactivity was measured. Nonspecific binding was defined as ligand binding in the presence of 10 μM unlabeled RaMH. Saturation experiments were conducted at five concentrations of [^{3}H]-RaMH from 5 to 500 nM by using PC12 cells infected with rAd-H3R (MOI = 2) and rAd-CLIC4 (MOI = 0 or 30). Curve fitting was made with GraphPad Prism version 4.00 (GraphPad Software Inc., USA).

Cell-based ELISA. CHO cells infected with rAd-H3R (MOI = 2) or rAd-H3RF419A (MOI = 2) and rAd-CLIC4 were seeded on collagen I-coated 24-well plates. Forty-eight hours after infection, cells were fixed in 4% PFA in PBS and blocked in PBS containing 5% fat-free milk. Cell surface H3R was detected with anti-H3R antibody, and HRP-conjugated anti-rabbit secondary antibody, followed by OPD colorimetric assay.

Wild-type CHO cells with no viral infection were used as negative control. To determine the total amount of H3R in cells, cells were permeabilized with 0.05% Tween 20 in PBS preceding the assay.

Results

Identification of CLIC4 as an H3R interacting protein

Screening of a human brain cDNA library with the C-terminus of H3R (amino acids 414–445) resulted in identification of a clone that harbored the coding sequence for amino acids 56–253 of CLIC4. To confirm the physical interaction of H3R with CLIC4, *in vitro* pull-down assays were performed with GST-H3R and MBP-CLIC4 fusion proteins. As shown in Fig. 1A, MBP-CLIC4 was coprecipitated strongly with GST-H3R C-terminus (414–445). While GST-H3R(414–436) also demonstrated strong interaction with MBP-CLIC4, other fusion proteins, GST-H3R(424–436), (414–423), and (421–427) showed no interaction. These results indicate that the 23 amino acid stretch from 414 to 436 of H3R is responsible for binding to CLIC4. As Chuang et al. showed that CLIC4 interacted also with the C-terminus of rhodopsin [12], we aligned the amino acid sequence 414–436 of H3R with that of the C-terminus of rhodopsin. The comparison showed that F419, R420 and K431 of H3R are shared with rhodopsin in comparable positions (Fig. 1B, upper panel). In order to see if these residues of H3R are involved in binding to CLIC4, we replaced each one or combinations of these residues with alanines. *In vitro* pull-down assays revealed that H3RF419A, FR/AA, and FRK/AAA completely lost the binding activities, indicating that F419 is critically important for H3R to interact with CLIC4 (Fig. 1B, lower panel). As for CLIC4, MBP-CLIC4 C-terminus (56–253) and MBP-CLIC4(121–253) interacted strongly with GST-H3R, but other subsegments of CLIC4 showed only minimum interactions with GST-H3R (Fig. 1C). These results indicate that the H3R binding domain of CLIC4 extends widely from amino acids 121 to 253.

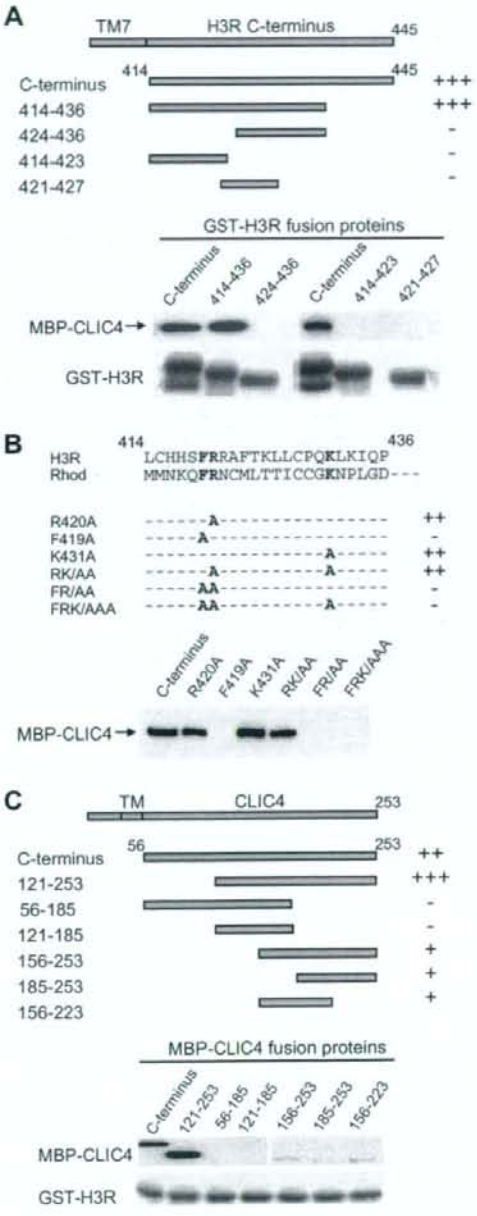

Fig. 1. Interaction of CLIC4 with H3R *in vitro*. Amino acid sequences responsible for the interaction between CLIC4 and H3R were determined. (A) Upper panel: Schematic diagram of full length C-terminal domain (414–445) and its distinct segments of H3R. Amino acid residue numbers, and binding activities with CLIC4 of each segment are indicated. Lower panel: Immunoblotting of MBP-CLIC4 coprecipitated with H3R and Coomassie blue staining of the samples. (B) Upper panel: Amino acid sequence alignment of H3R414–436 and C-terminus of rhodopsin (GenBank Accession Nos. NM_007232 and NM_000539). Boldface letters show amino acid residues replaced with alanines to generate mutant forms of H3R. Activities of each mutant to bind CLIC4 are indicated. Lower panel: Immunoblotting of MBP-CLIC4 coprecipitated with each mutant of GST-H3R. (C) Mapping of active subdomain of CLIC4 interacting with H3R. Upper panel: Schematic illustration of CLIC4(56–253) and its subsegments with their binding activities to H3R C-terminus. Lower panel: Immunoblotting detection of MBP-CLIC4 coprecipitated with H3R C-terminus, and Coomassie blue staining of the samples.

In vivo association of CLIC4 with H3R

The association of CLIC4 with H3R was studied in PC12 cells transiently expressing both H3R and CLIC4. Immunofluorescence microscopy showed overlapping localizations of the two proteins at the plasma membrane (Fig. 2A). Then, immunoprecipitation experiments using P2 fraction of rat brain homogenates revealed that endogenous CLIC4 was coimmunoprecipitated with H3R

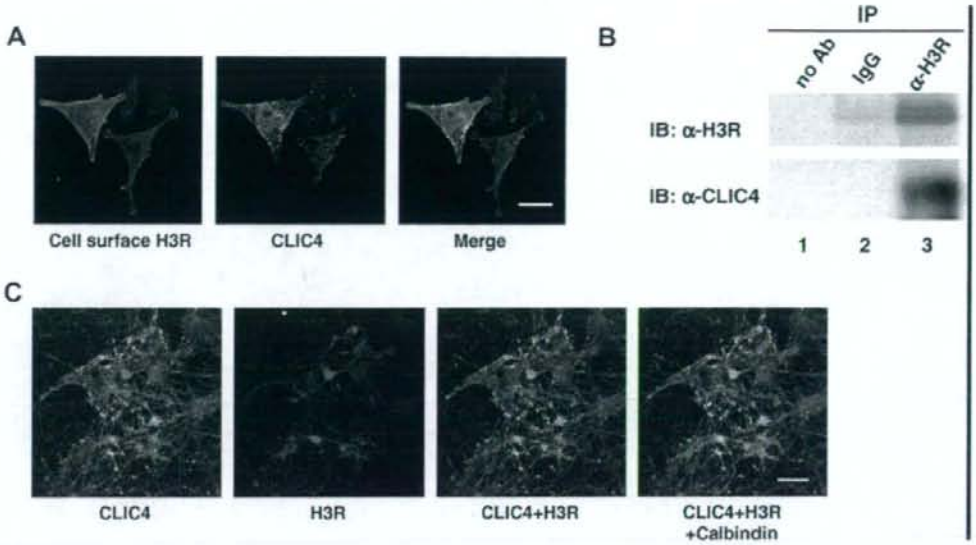

Fig. 2. *In vivo* association of CLIC4 with H3R. (A) Colocalization of CLIC4 and H3R at the plasma membrane of PC12 cells. Regions of colocalization of surface H3R and CLIC4 appear yellow in the merged image. Scale bar: 10 μm. (B) Coimmunoprecipitation of endogenous CLIC4 with H3R. Solubilized proteins from rat brain P2 fraction were immunoprecipitated with no antibody (lane 1), irrelevant IgG (lane 2), or anti-H3R antibody (lane 3) and probed with anti-H3R or anti-CLIC4 antibodies. (C) Distribution of endogenous CLIC4 and H3R in rat cerebellar Purkinje cells. Cells were stained for H3R, CLIC4, and calbindin D-28K, a Purkinje cell-specific marker. Regions of colocalization of H3R and CLIC4 appear yellow and triple colocalization areas appear white in the merged image. Scale bar: 50 μm.

(Fig. 2B). Furthermore, in immunofluorescence analysis of primary culture of rat cerebellar neurons, endogenous CLIC4 and H3R were colocalized in cell bodies and dendrites of Purkinje cells (Fig. 2C). These observations demonstrate that CLIC4 associates with H3R in native cells.

CLIC4 promotes cell surface expression of H3 receptor

To see whether CLIC4 alters the H3R trafficking in cells, cell surface H3R expression was examined by flow cytometry. PC12 cells were coinfected with rAd-H3R and rAd-CLIC4, and cell surface H3R-derived fluorescence signals were measured. Fluorescence intensity was increased dose-dependently with simultaneous introduction of CLIC4 (Fig. 3A), indicating that increasing number of H3R was expressed on cell surface with the coexpression of CLIC4. Fluorescence signals measured in permeabilized cells indicated that the total amount of H3R in cells was not affected by CLIC4 (data not shown). We next investigated whether binding site of H3R specific ligand was altered by CLIC4. The [^{3}H]-RaMH specific binding showed progressive increase depending on the amount of rAd-CLIC4 used to infect the cells (Fig. 3B). We next performed saturation binding experiments with the radioligand. Scatchard plot analysis indicated that cells expressing H3R alone showed a single low-affinity binding site with a K_d value of 44.43 nM and a B_{max} value of 10.57 fmol/cell (Fig. 3C). On the other hand, cells expressing both H3R and CLIC4 displayed two distinct affinity sites with K_d values of 0.99 nM and 94.55 nM, and B_{max} values of 2.71 fmol/cell and 17.24 fmol/cell for high- and low-affinity sites, respectively. Although the K_d value at the low-affinity sites has decreased more than 50% (from 44.43 nM to 94.55 nM), CLIC4 expression revealed new high-affinity sites on cells (K_d value of 0.99 nM) and increased nearly twice the total binding site density on cells (from 10.57 fmol/cell to 19.95 fmol/cell). We also investigated whether CLIC4 expression would influence cell surface expression of H3R in a different type of cells. Cell-based ELISA using CHO cells showed that cell surface expression of H3R was enhanced dose-dependently with simultaneous introduction of CLIC4 (Fig. 4A). It should be noted that the total amount of H3R detected in permeabilized cells was not influenced by CLIC4 (data not shown). This result indicates that the effect of CLIC4 is not restricted to a particular cell type but rather a more general attribute of CLIC4 to promote cell surface expression of H3R.

Surface expression of a mutant H3R is not enhanced by CLIC4

To confirm whether the specific interaction between H3R and CLIC4 is required for the increase in cell surface expression of the receptor, we investigated the effect of CLIC4 on the F419A mutant form of H3R that failed to interact with CLIC4. As demonstrated in Fig. 4B, the H3RF419A cell surface expression was

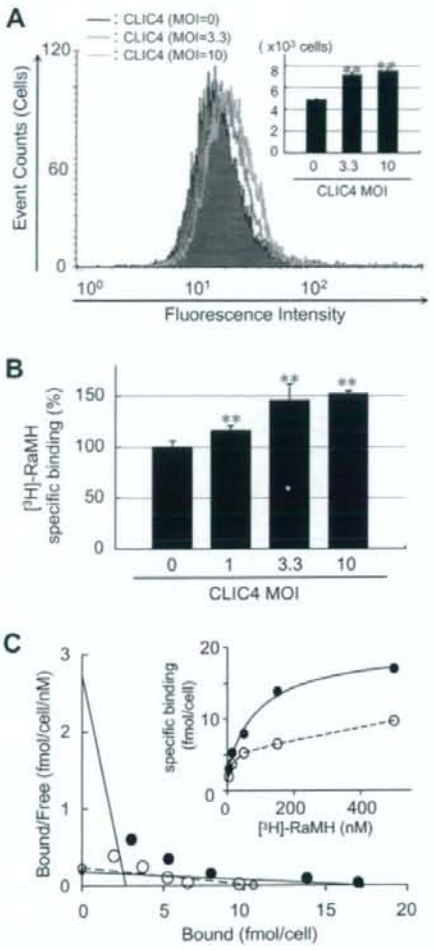

Fig. 3. Enhancement of H3R cell surface expression by CLIC4. (A) Effects of CLIC4 on H3R cell surface expression analyzed by flow cytometry. FACS analysis shows that fluorescence intensity derived from cell surface H3R was shifted to the right dose-dependently with simultaneous introduction of CLIC4. The inset shows a histogram of number of fluorescence-positive cells in each cell population. Data are shown in means ± SE of three independent experiments. $^{**}p < 0.01$ versus control. (B) Radioligand receptor assay. Specific binding of [^{3}H]-RaMH was measured in PC12 cells coinfected with rAd-H3R and rAd-CLIC4. Values were normalized to [^{3}H]-RaMH binding to cells infected with only rAd-H3R. Each column represents the mean ± S.E. of three independent experiments. $^{**}p < 0.01$ versus control. (C) Scatchard plot of radioligand binding to H3R. Open circles indicate data from cells infected with only rAd-H3R. Closed circles denote cells coinfected with rAd-H3R and rAd-CLIC4. The inset shows the saturation curve of [^{3}H]-RaMH binding to the cells. Data are means of triplicate determinations.

not influenced by CLIC4. Basal level cell surface expression of the F419A mutant was comparable to that of the wild-type receptor (data not shown). This result strongly supports the idea that H3R cell surface expression enhanced by CLIC4 is caused by the specific interaction of H3R with CLIC4.

Discussion

Biosynthesis and fate of GPCRs are tightly coupled to the process of their trafficking within cells. After synthesized at ER, properly folded GPCRs are packaged into ER-derived vesicles and then conveyed to cell surface along the way through Golgi apparatus and trans-Golgi network (TGN). During the course of the transit to cell surface, GPCR molecules are post-translationally modified and assembled with effector signaling molecules including heterotrimeric G proteins. At the plasma membrane, GPCRs stimulated by their cognate ligands undergo internalization. Internalized receptors are carried through endosomes and then either degraded in lysosomes or recycled back to the plasma membrane. The number of GPCR molecules on the plasma membrane is defined by the balance of these processes of intracellular trafficking of the receptor. As H3R has been known to exhibit high constitutive activity [14], the receptor would be constitutively internalized even in steady state without ligand stimulation and recycled or degraded within cells. The ability of CLIC4 to enhance cell surface expression of H3R could, therefore, be explained by one or combinations of the following mechanisms: increase of forward trafficking of H3R from ER to cell surface, inhibition of constitutive receptor internalization, and increase of the receptor recycling back to the plasma membrane. CLIC4 is reported to interact with dynamin I [11], a protein essential in endocytosis. It is tempting, therefore, to speculate that CLIC4 expression would somehow influence activities of dynamin I, causing inhibition of the receptor internalization. As for the receptor recycling, endosome acidification is mandatory to maintain efficient vesicle recycling [15]. Proton transport required for the acidification of the endosomes should be balanced electrochemically with a concurrent chloride conductance of the vesicle membranes. Therefore, it would be conceivable that CLIC4 provides this conductance and enhances the recycling process of the constitutive active H3R. The third mechanism, increase of the forward trafficking of H3R, would also play a role in enhancing cell surface expression of the receptor.

Extensive studies on trafficking of GPCR have led to the identification of the structural determinants on the C-terminus of GPCR that dictate the efficiency of exit of the receptor from ER [16]. Among the several consensus motifs reported so far, $F(X)_6LL$ (where X can be any residues and L is leucine or isoleucine) conforms to the CLIC4 binding site of H3R. The motif is reported to allow α_{2B}-adrenergic (α_{2B}-AR) and angiotensin II type 1 (AT1R) receptors to exit from ER [17]. The report also signifies the importance of the phenylalanine in this motif by showing that replacement of the residue with alanine causes both receptors to be unable to exit from ER. Because F419 of H3R is also critical for responding to CLIC4 enhancement of the receptor cell surface expression, it is intriguing to speculate that the protein responsible for binding this motif and assisting these receptors to exit from ER is CLIC4. However, a noticeable difference of H3R is that, unlike those mutants